Proceeding of the LHC Seminar "Updated angular analysis of the decay $B^0 \to K^{\star 0}\,(\to K^+\pi^-)\,\mu^+\mu^-$" held by Eluned Anne Smith

Nicole Schulte
Technische Universität Dortmund
(Dated: August 13, 2020)

The LHC seminar [1] discusses the updated angular analysis from the LHCb collaboration of the decay channel $B^0 \to K^{\star 0}\,(\to K^+\pi^-)\,\mu^+\mu^-$ adding 2016 data recorded in proton-proton collisions at the LHC to the previous analysis. The recorded data corresponds to an integrated luminosity of $\mathcal{L} = 4.9\,\mathrm{fb}^{-1}$. The full analysis includes the 2016 data, Run1 data and a combination. The local tension in the angular observable $P_5^{'}$ as a function of the dimuon mass is analysed in various bins. Compared to the previous analysis, the significance of the local tension diminishes, but the overall tension becomes stronger. The combined dataset indicates that a shift in the Wilson coefficient $\mathcal{C}_9$ with a significance of 3.3σ might be responsible for the local tension but could also be interpreted as a statistical fluctuation. The complete set of measurements into the $b \to s\mu^+\mu^-$ transition performed by various experiments includes the observables R_K and $R_K^\star$, describing ratios corresponding to $B \to K^{(\star)}ll$ decays involving muons and electrons. This analysis focusses on observables in the P_i and S_i basis and does not include R_K and $R_K^\star$.

I. EFFECTIVE DESCRIPTION OF THE DECAY

The decay of the pseudoscalar B^0-meson to the $K^{\star 0}$-vector-meson can be described with the flavor-changing neutral current $b \to s\mu^+\mu^-$ transition displayed in Figure 1. In the Standard Model, this process is suppressed at loop-level due to the GIM-Mechanism and forbidden at tree-level due to flavor-changing neutral currents (FCNCs). Therefore the decay is loop-suppressed in the Standard Model and can be categorized as a rare decay. These rare decays are more sensitive to new physics than processes without major loop-level contributions because they have a smaller branching fraction and can involve new particles such as leptoquarks and other virtual contributions from new particles. These contributions of new physics particles in indirect searches lead to higher energy scales that affect the branching ratio. Direct searches are not able to access these high energies, therefore a indirect search is used.

The $b \to s\mu^+\mu^-$ transition is described with an effective field theory. The heavier degrees of freedom from loop-contributions are factorized out and replaced with an effective coupling, the Wilson coefficients. The decay involving a Z^0-boson can be described with two effective couplings describing the vector and axial-vector part of the gauge boson respectively. These Wilson coefficients are denoted $\mathcal{C}_9$ for the vector coupling and $\mathcal{C}_{10}$ for the axial-vector coupling. The decay involving a photon can be discribed with only one effective coupling, denoted as $\mathcal{C}_7$. The Wilson coefficients are sensitive to new physics because they describe the loop-contribution of the higher-level diagrams. In the effective Hamiltonian,

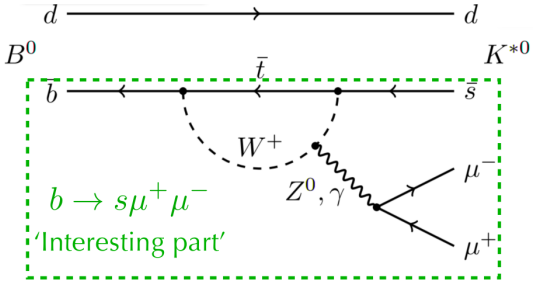

FIG. 1: Standard Model Feynman diagram displaying the $b \to s\mu^+\mu^-$ transition in the $B^0 \to K^{\star 0}\,(\to K^+\pi^-)\,\mu^+\mu^-$ decay. The green box surrounds the part of the diagram that can be described in new physics models replacing the loop with an effective coupling [1].

$$H_{\text{eff}} = -\frac{4G_F}{\sqrt{2}} V_{tb}V_{ts}^\star \sum_i \left(\mathcal{C}_i\mathcal{O}_i + \mathcal{C}_i'\mathcal{O}_i'\right) ,$$

the Wilson coefficients are combined with operators $\mathcal{O}_i$ which describe non-perturbative quantum chromodynamics (QCD) as well as the low energy contribution of the Feynman diagram. The effective Hamiltonian includes the CKM-matrix elements V_{tb} and V_{ts}, describing the mixing between a top-quark and either a b-quark or a s-quark, as well as Fermi's constant G_F. The operators carry a large theory uncertainty because their description involves formfactors which require theoretical modelling.

By performing an angular analysis, theoretical uncertainties are reduced. Angles can be described as rotations in phase space and therefore the measurement of the decay rate as a function of the angles of the decay product opens up the possibility to contruct experimental observables less dependent on theoretical modelling. In this decay an angular analysis is useful because the three polarisations of the $K^{\star 0}$ provide a rich angular structure and more angular observables can be extracted.

II. PREVIOUS MEASUREMENT FROM RUN1

The previous measurement used data corresponding to an integrated luminosity of $\mathcal{L} = 3\,\mathrm{fb}^{-1}$ recorded at the

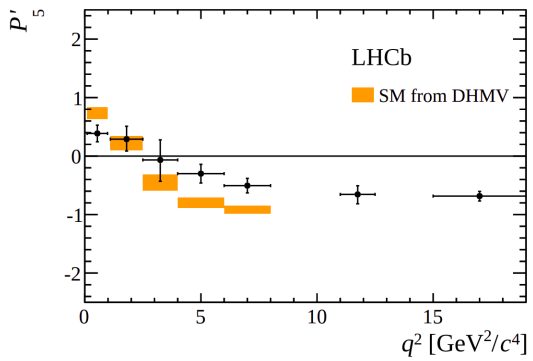

FIG. 2: The value $P_5^{'}$ as a function of the dimuon mass. Using Run1 data local tension of the data (black dots) and the Standard Model prediction (orange areas) can be found in fourth and fifth bin [2].

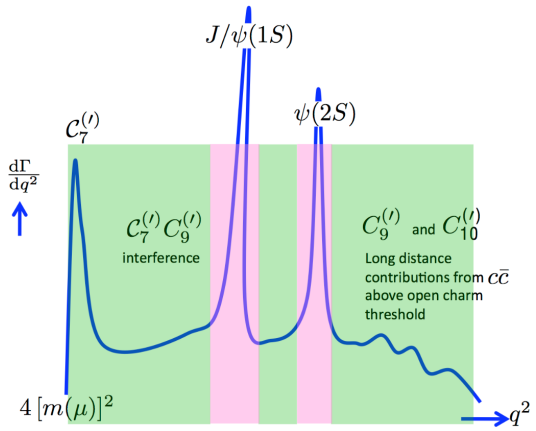

FIG. 3: Areas with major charmonium resonances (red) that are removed for the analysis. Areas displayed in green are used as signal regions in the q^2 mass spectrum [1].

LHC in Run1 at a centre-of-mass energy of $\sqrt{s} = 7\,\text{TeV}$ and $\sqrt{s} = 8\,\text{TeV}$. Figure 2 displays the angular observable $P_5^{'}$ as a function of the dimuon mass q^2. The angular observables are determined from a maximum likelihood fit to the invariant mass $m\,(K^+\pi^-\mu^+\mu^-)$ and the decay angles $\cos\theta_l$, $\cos\theta_K$ and ϕ in each bin of q^2 [2]. The angles are described in more detail in Section III. In the bins $4.0{<}q^2{<}6.0\,\text{GeV}^2/c^4$ and $6.0{<}q^2{<}8.0\,\text{GeV}^2/c^4$ local tension between the data and the Standard Model predition can be found with a significance of 3.0σ.

The overall shift in the Wilson coefficient $\mathcal{C}_9$ that would be needed to explain the tension displayed in Figure 2 would be 3.4σ from the Standard Model prediction assuming only a shift in $\mathcal{C}_9$ could explain the observation. The overall shift in the vector-coupling strength with the significance for Run1 data is included in Figure 6 as a dashed blue line, using a fit to the results of a maximum likelihood fit of the CP-averaged observables. Averaging over CP means that both B^0 and $\bar{B}^0$ decays are included reducing the uncertainty as K^+ and K^--mesons interact differently in the detector.

Global fits performed by various experiments i.e. Belle and ATLAS to a complete set of $b \to sll$ measurements measured a significance of $3 \to 5\sigma$ in the Wilson coefficients in respect to the Standard Model. The complete set of measurements includes, but it not limited to, measurements into the ratio $R_K = \frac{\mathcal{B}(B\to K\mu^+\mu-)}{\mathcal{B}(B\to Ke^+e^-)}$ probing lepton-flavor-universality (LFU) and $R_K^\star$ the LFU-violating ratio corresponging to $B \to K^\star l^+ l^-$ [3].

III. ANALYSIS TECHNIQUES

In the event selection, two muon candidates, a kaon and a pion are required. The Impact Parameter (IP) is used to distinguish between B-mesons originating from the primary vertex and the muons, kaons and pions which do not originate from the primary vertex. The peaking background originates from the misidentification of other particles as one of the required candidates is measured by particle information from the RICH detectors. The background from incorrecly vertexed tracks, the combinatorial background, is suppressed by using machine learning techniques. Boosted decision tree (BDT) algorithms [4] are used as machine learning technique. Input variables for the BDT are the reconstructed B^0 decay-time and vertex-fit quality, momentum and transverse momentum of the B^0 candidate, θ_{DIRA}, particle identification information from the RICH detectors and the muon chambers and variables describing the isolation of the final state tracks [5]. The variable θ_{DIRA} describes the angle between the reconstructed B^0 momentum and the vector connecting the primary vertex to the reconstructed B^0 decay vertex and is required to be small. The input variables are required to have no correlation with the decay angles θ_l, θ_K and ϕ or q^2. The BDT is trained on data with $B^0 \to J/\psi K^{\star 0}$ candidates as a substitute for the signal and for the background, candidates from the upper-mass sideband $5350{<}m\,(K^+\pi^-\mu^+\mu^-){<}7000\,\text{MeV}/c^2$ are used.

Regions in the dimuon spectrums are removed to avoid major background from charmonium resonances as displayed in Figure 3. The charmonium background produces the same final state, therefore areas where this background peaks cannot be considered for the analysis. Short distance physics in the dimuon spectrum has no resonant structure and is smaller than the peaking areas of the charmonium background. The area, where the J/ψ peaks is used as a control channel as the statistics in this channel is higher than in the rare mode.

By adding the 2016 data to the Run1 data, the number of signal candidates will be about twice as high as the signal cross section rises with higher centre-of-mass energies and the number of events scales proportianally to the cross section. After excluding the charmonium and

light resonance regions the remaining background is only combinatorial.

Three angles are needed to describe the decay: θ_l as the angle between $\mu^+\,(\mu^-)$ and direction opposite to that of the $B^0\,(\bar{B}^0)$ in the rest frame of the dimon system, θ_K as the angle between $K^+\,(K^-)$ and $B^0\,(\bar{B}^0)$ in the rest frame of the $K^{\star 0}\,(\bar{K}^{\star 0})$ system and ϕ as the angle between the plane defined by the dimuon pair and the plane defined by the kaon and pion in the $B^0\,(\bar{B}^0)$ rest frame. The decay rate can then be described by the sum of the angular functions $f_i\left(\vec{\Omega}\right)$, depending on the three angles times the angular coefficients $I_i\left(q^2\right)$, depending on the dimuon mass according to

$$\frac{\mathrm{d}^4\Gamma\left[\bar{B}^0 \to \bar{K}^{\star 0}\mu^+\mu^-\right]}{\mathrm{d}q^2\mathrm{d}\vec{\Omega}} = \frac{9}{32\pi}\sum_i I_i\left(q^2\right) f_i\left(\vec{\Omega}\right) .$$

The angular coefficients are bilinear combinations of the $K^{\star 0}$ amplitudes. The amplitudes originate from the three different polarisations of the $K^{\star 0}$ and are dependant on the Wilson coefficients and the form factors. In example, the angular coefficient I_1^s is denoted as

$$I_1^s = \frac{3}{4}\left[|A_\parallel^{\mathrm{L}}|^2 + |A_\perp^{\mathrm{L}}|^2 + |A_\parallel^{\mathrm{R}}|^2 + |A_\perp^{\mathrm{R}}|^2\right]$$

with the corresponding angular function $f_1^s\left(\theta_K\right) = \sin^2\theta_K$. One of these $K^{\star 0}$ amplitudes is defined as

$$A_\perp^{\mathrm{L(R)}} = \mathcal{N}\sqrt{2\lambda}\left\{\left[\left(\mathcal{C}_9^{\mathrm{eff}} + \mathcal{C}_9^{\prime\mathrm{eff}}\right) \mp \left(\mathcal{C}_{10}^{\mathrm{eff}} + \mathcal{C}_{10}^{\prime\mathrm{eff}}\right)\right.\right.$$
$$\left.\left.\frac{V\left(q^2\right)}{m_B + m_{K^\star}} + \frac{2m_b}{q^2}\left(\mathcal{C}_7^{\mathrm{eff}} + \mathcal{C}_7^{\prime\mathrm{eff}}\right) T_1\left(q^2\right)\right]\right\}$$

including the Wilson coefficients $\mathcal{C}_{7,9,10}$ and the form factors $V\left(q^2\right)$ and $T_1\left(q^2\right)$. Form factors originate from theoretical modelling and therefore carry a theoretical uncertainty. By constructing ratios of these observables, the dependence on the form factors can cancel out.

A. The Angular Fit

The analysis is performed in different bins of the dimuon mass. First, an integration over the dimuon mass is performed, than the B^0 and $\bar{B}^0$ decays are combined leading to CP-average observables. This leads to eight CP-averaged observables that can be extracted from the fit of the invariant mass of the decay products in each bin of q^2. This is denoted as the S_i basis [2] with

$$S_i = \left(I_i + \bar{I}_i\right) / \left(\frac{\mathrm{d}\Gamma}{\mathrm{d}q^2} + \frac{\mathrm{d}\bar{\Gamma}}{\mathrm{d}q^2}\right) .$$

The amount of the longitudinally polarised $K^{\star 0}$s as well as the forward-backward asymmetry of the dimuon system are also considered for the S_i basis.

In the $P_i^{'}$ basis, ratios of the observables from the S_i basis are constructed to cancel uncertainties from form factors at first order. This results in seven CP-averaged observables in this basis that can be extracted from the fit of the invariant mass of the decay products in each bin of q^2. As an example, the $P_5^\prime$ definition is given because the local tension in this variable is displayed in the analysis:

$$P_5^\prime = \frac{S_5}{\sqrt{F_L\left(1 - F_L\right)}} .$$

The fit is performed twice in the S_i basis and once in the optimised $P_i^{'}$ basis.

In order to obtain the total probability density function (PDF), mass shapes are used to determine the fraction of the signal and background contributions. A maximum likelihood fit on the total PDF is performed. A gaussian function is used to described the signal and a polynomial as well as an exponential function are used to describe the combinatorial background. The 2016 and Run1 data are fitted simultaneously because they do not share the same mass and angular background components because the conditions in Run1 and 2016 data were different and resolution effects and similar effects are contributing factors.

The efficiency does not provide a flat behaviour, therefore a correction is needed. For each data set, the efficiency is calculated using Legendre polynomials for the three angles and the dimuon mass. The 4D formular can not be reduced to four seperate one-dimensional formulas, as the observables are correlated and can therefore not be factorized.

The desired candidates are $K^{\star 0}$s with spin 1 in the P-wave configuration in the $P_i^{'}$ basis. Underlying resonances in the spin zero configuration need to be removed. These resonances are denoted as the S-wave. The angular distribution of the S-wave is considered in the fit with the fraction of the S-wave candidates and interference terms between the two waves. The invariant mass of the Kaon and pion system is used to contrain the S-wave, because both waves have distinct line shapes in this distribution.

Every basis has different dominant systematic uncertainties. In the $P_i^{'}$ basis the acceptance variation with the dimuon mass accounts for the dominant systematic uncertainty. In the S_i basis, the peaking background dominates. All systematic uncertainties are small compared to statistical errors. Bias corrections are performed to minimise the bias from boundary effects.

IV. RESULTS

Comparing the results from Run1 with the results using 2016 data and the combination of both an agreement between both analyses can be found in the S_i basis. The results corresponding to 2016 only data is used only for illustrative purposes as it contains no systematic uncertainties or bias and coverage corrections. The most interesting analysis results are from the combination of both data sets.

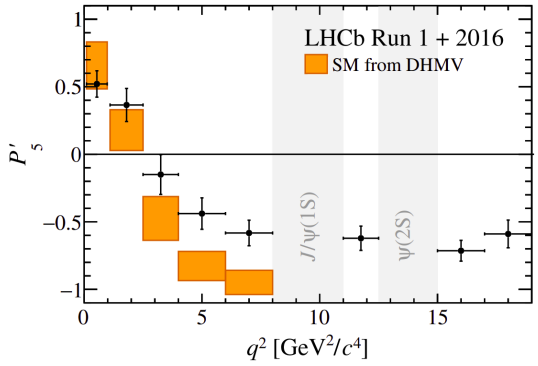

FIG. 4: The CP-averaged angular observable $P_5^{'}$ as a function of the dimuon mass. Compared to the Standard Model prediction, local tension can be found in the fourth and fifth bin using 2016 and Run1 data combined [6].

Figure 4 displays the angular observable $P_5^{'}$ as a function of the dimuon mass. Compared to the Run1 results from Figure 2, the local tensions in the $4.0{<}q^2{<}6.0\,\mathrm{GeV}^2/c^4$ and $6.0{<}q^2{<}8.0\,\mathrm{GeV}^2/c^4$ bins remain with a significance of 2.5σ and 2.9σ respectively. The local tension for both data sets combined is reduced compared to the Run1 analysis.

To obtain the global significance, all observables in the S_i basis need to be fitted to the complete set of CP-averaged observables obtaines from the maximum likelihood fit from the invariant mass of the system of the decay products including all bins of q^2 and the Wilson coefficients need to be extracted. Compared to previous publications, the theory uncertainty associated with form factors has decreased and the parametrisation of sub-leading corrections has become more conservative. The global fit consideres two cases. In the first case, the same dimuon range as before is used. Narrow bins below $q^2{<}8\,\mathrm{GeV}^2/c^4$ and wide bins between $15.0{<}q^2{<}19.0\,\mathrm{GeV}^2/c^4$ are considered. In the second case the bin $6.0{<}q^2{<}8.0\,\mathrm{GeV}^2/c^4$ is removed additionally as it is very close to the J/ψ region leading to sub-leading correction issues.

A shift in the Wilson coefficient $\mathcal{C}_9$ is measured in the varation of the real part of both $\mathcal{C}_9$ and $\mathcal{C}_{10}$ in agreement to the Run1 results as displayed in Figure 5. The shift in the Wilson coefficient by only varying $\mathcal{C}_9$ is displayed in Figure 6. It can be seen, that the Run1 analysis is in good agreement with the 2016 analysis. The significance including the $6.0{<}q^2{<}8.0\,\mathrm{GeV}^2/c^4$ bin for the combination of 2016 and Run1 is 3.3σ and 2.4σ when excluding the bin.

Figure 7 displays the angular observable $P_5^{'}$ as a function of the dimuon mass. Included is theoretical prediction for two variations of the prefered Wilson coefficient $\mathcal{C}_9$. The predictions close the gap between the Standard Model prediction and the combined data, reducing the local tension.

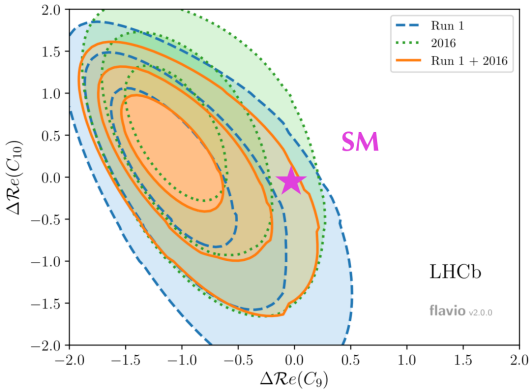

FIG. 5: Prefered shift in the real part of $\mathcal{C}_9$ and $\mathcal{C}_{10}$ compared to the Standard Model value [1].

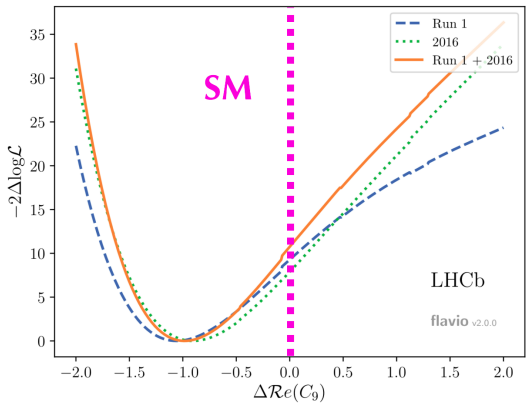

FIG. 6: Prefered shift in the real part of $\mathcal{C}_9$ obtained from the analysis compared to the Standard Model value. All data sets are in good agreement [1].

Concluding, the results presented in the seminar support the overall tension that has been hinted in Run1 data from previous measurements and publications. Although the local tension is less evident than previously and the overall tension is higher, it can not be stated that new physics has been found, only hinted. Including more data from other experiments like Belle probing new physics at different scales could strengthen these hints. The $b \to s$ transition can also be studied in B decays mediated by $b \to s\gamma$ [7] in addition to the $b \to sl^+l^-$ analysis, presented in the seminar. In addition to angular observables, measurements in the ratios R_K and $R_K^\star$ are also performed [3]. Angular analysis are important as new physics can be probed at higher scales and due to the optimised basis, theoretical uncertainties originating from form factors can be reduced.

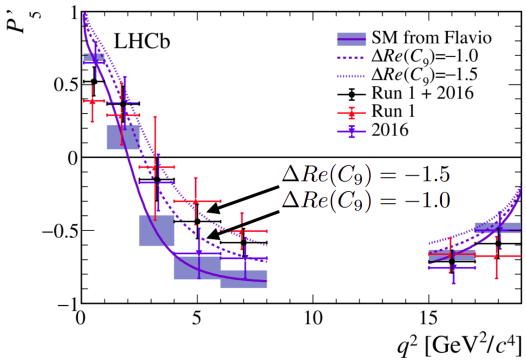

FIG. 7: Angular observable $P_5^{'}$ as a function of the dimuon mass. The Standard Model prediction as well as theoretical predictions with a shifted Wilson coefficient are included [1].

[1] E. A. Smith, Updated angular analysis of the decay $B^0 \to K^{*0}(\to K^+\pi^-)\mu^+\mu^-$. Updated angular analysis of the decay $B^0 \to K^{*0}(\to K^+\pi^-)\mu^+\mu^-$, (2020).

[2] R. Aaij *et al.* (LHCb), Angular analysis of the $B^0 \to K^{*0}\mu^+\mu^-$ decay using 3 fb^{-1} of integrated luminosity, JHEP **02**, 104, arXiv:1512.04442 [hep-ex].

[3] A. K. Alok, A. Dighe, S. Gangal, and D. Kumar, Continuing search for new physics in $b \to s\mu\mu$ decays: two operators at a time, JHEP **06**, 089, arXiv:1903.09617 [hep-ph].

[4] Y. Freund and R. E. Schapire, A decision-theoretic generalization of on-line learning and an application to boosting, Journal of Computer and System Sciences **55**, 119 (1997).

[5] R. Aaij *et al.* (LHCb), Measurement of *CP*-averaged observables in the $B^0 \to K^{*0}\mu^+\mu^-$ decay, Phys. Rev. Lett. **125**, 011802 (2020), arXiv:2003.04831 [hep-ex].

[6] S. Descotes-Genon, L. Hofer, J. Matias, and J. Virto, On the impact of power corrections in the prediction of $B \to K^*\mu^+\mu^-$ observables, JHEP **12**, 125, arXiv:1407.8526 [hep-ph].

[7] F. Beaujean, C. Bobeth, and D. van Dyk, Comprehensive bayesian analysis of rare (semi)leptonic and radiative b decays, The European Physical Journal C **74**, 10.1140/epjc/s10052-014-2897-0 (2014).

[8] J. Aebischer, W. Altmannshofer, D. Guadagnoli, M. Reboud, P. Stangl, and D. M. Straub, B-decay discrepancies after Moriond 2019, Eur. Phys. J. C **80**, 252 (2020), arXiv:1903.10434 [hep-ph].

[9] J. Alves, A.Augusto *et al.* (LHCb), The LHCb Detector at the LHC, JINST **3**, S08005.